ADVANCED FUNCTIONAL MATERIALS
www.afm-journal.de

Mesoporous Silica Coated Single-Walled Carbon Nanotubes as a Multifunctional Light-Responsive Platform for Cancer Combination Therapy

*Jingjing Liu, Chao Wang, Xiaojing Wang, Xin Wang, Liang Cheng, Yonggang Li, and Zhuang Liu**

The development of cancer combination therapies, many of which rely on nanoscale theranostic agents, has received increasing attention in recent years. In this work, polyethylene glycol (PEG) modified mesoporous silica (MS) coated single-walled carbon nanotubes (SWNTs) are fabricated and utilized as a multifunctional platform for imaging guided combination therapy of cancer. A model chemotherapy drug, doxorubicin (DOX), could be loaded into the mesoporous structure of the obtained SWNT@MS-PEG nano-carriers with high efficiency. Upon stimulation under near-infrared (NIR) light, photothermally triggered drug release from DOX loaded SWNT@MS-PEG is observed inside cells, resulting in a synergistic cancer cell killing effect. As revealed by both photoacoustic (PA) and magnetic resonance (MR) imaging, we further uncover efficient tumor accumulation of SWNT@MS-PEG/DOX after intravenous injection into mice. In vivo combination therapy using this agent is further demonstrated in a mouse tumor model, achieving a remarkable synergistic anti-tumor effect superior to that obtained by mono-therapy. Our work presents a new type of theranostic nano-platform, which could load therapeutic molecules with high efficiency, be responsive to external NIR stimulation, and at the same time serve as a diagnostic imaging agent.

1. Introduction

Chemotherapy is a general therapeutic approach for the treatment of a wide variety of cancers.[1] Despite tremendous efforts in the development of various nanoparticle-based drug delivery systems (DDSs), how to specifically control the release of therapeutics at the desired lesions (e.g., tumors), and improve the therapeutic efficacy of chemotherapy remain an important task that merits further investigations. Designing multifunctional DDSs, which are responsive to external physical stimuli and able to deliver combination therapy for more effective cancer treatment, has thus received significant interest in the area of nanomedicine.[2]

Mesoporous silica nanoparticles (MSNs) with many unique characteristics including large surface area, high pore volume, tunable nanometer-scale pore sizes, abundant inner/outer surface chemistries and intrinsic biocompatibility,[3] have attracted great attention as a versatile DDS platform. To date, several stimulus-responsive strategies employing light irradiation,[4] pH,[5] temperature,[6] enzymes,[7] and redox activation[8] as "triggers" have been developed to fabricate smart MSN-based DDSs, aiming at precisely controlling drug release at desired localizations / timings. Among those nanoscale platforms, encapsulating near-infrared (NIR) light-absorbing nanoparticles, which include gold nanorods (AuNRs),[9–11] graphene nanosheets,[12] copper chalcogenides (Cu_9S_5)[13] and many others, inside mesoporous silica has been proposed to be a general approach to realize combined photothermal & chemotherapy. In those systems, photothermal heating of the core nanoparticle under NIR laser usually would trigger release of drug molecules loaded inside the mesoporous silica shell, resulting in enhanced cancer cell killing.

Single-walled carbon nanotubes (SWNTs) with many interesting physical and chemical properties have been extensively explored in the area of nanomedicine.[14–16] As one of the "darkest" materials in the world, SWNTs exhibit strong optical absorption from visible to NIR regions, making them a robust photothermal agent for effective tumor ablation.[17] Many research groups have also utilized the intrinsic physical properties of SWNTs for multimodal biomedical imaging.[15,18] However, although many methods have been reported to prepare silica coated carbon nanotubes,[19,20] the development of mesoporous silica (MS) coated SWNTs as a light-responsive drug delivery platform for combination therapy of cancer has not yet been explored to our best knowledge.

In this work, MS coated SWNTs are fabricated and then further functionalized with polyethylene glycol (PEG) to acquire enhanced solubility and stability in physiological environments.

J. J. Liu, C. Wang, X. J. Wang,
Dr. L. Cheng, Prof. Z. Liu
Institute of Functional Nano & Soft Materials (FUNSOM)
Collaborative Innovation Center of Suzhou Nano Science and Technology
Soochow University
Suzhou, Jiangsu 215123, China
E-mail: zliu@suda.edu.cn
X. Wang, Prof. Y. G. Li
Department of Radiology
the First Affiliated Hospital of Soochow University
Suzhou, Jiangsu 215006, China

DOI: 10.1002/adfm.201403079

An anti-cancer drug, doxorubicin (DOX) can be loaded into the mesoporous structure of the obtained SWNT@MS-PEG nanocarrier with high efficiency. Compared with PEGylated SWNTs with direct DOX adsorption and no MS shell, the drug release of our newly developed SWNT@MS-PEG/DOX appears to be much more sensitive to light stimulation. Owing to the photothermally accelerated cellular uptake of nano-carriers and the light-triggered drug release inside cells, synergistic cancer cell killing effect is then realized by combined photothermal and chemotherapy. With strong NIR absorbance and metallic nanoparticles decorated on their surface, SWNTs are able to offer contrast in both photoacoustic (PA) and magnetic resonance (MR) imaging,[21] which uncover efficient tumor accumulation of SWNT@MS-PEG/DOX after intravenous injection into tumor-bearing mice. In vivo combination therapy is finally carried out with SWNT@MS-PEG/DOX, demonstrating outstanding tumor-suppression effect by only a single treatment using a relatively low drug dosage and laser power density. Therefore, MS coated SWNTs with PEG coating appear to be an interesting class of theranostic platform useful for imaging-guided combination therapy of cancer.

2. Results and Discussion

The strategy for synthesis of mesoporous silica coated SWNTs is shown in **Figure 1**a. Raw SWNTs were firstly solubilized by a cationic surfactant cetyl-methyl-ammonium bromide (CTAB). When tetraethyl orthosilicate (TEOS) was injected into the obtained SWNT/CTAB solution, it was hydrolyzed and condensed into silicate polyanions, which interacted with the surface of positively charged SWNTs with CTAB coating. A silica shell was then formed surrounding each SWNT after further hydrolyzation of silicate. After washing with ethanol to remove CTAB, which served as the mesostructural template, mesoporous silica coated SWNTs (SWNT@MS) were obtained. Finally, the SWNT@MS composite was modified subsequently with octadecyltrimethoxysilane (C18TMS) and then PEG-grafted poly (maleic anhydride-alt-1-octadecene) (C18PMH-PEG), obtaining PEGylated SWNT@MS (SWNT@MS-PEG) with great water solubility. Transmission electron microscopy (TEM) images (Figure 1b and Supporting Information Figure S1a) of SWNT@MS revealed that a mesoporous silica shell with from the thickness of 15 to 25 nm was formed around SWNTs, whose lengths ranged from 100 to 300 nm. Hardly any free SiO_2 particles were found in the TEM view. As shown in the high-resolution TEM image, the pores were perpendicular to the surface of SWNTs. This kind of feature would facilitate the mass transportation between the inner and outer surfaces of the silica coating to allow drug loading and release. The surface area, pore volume, and average pore diameter of SWNT@MS were determined to be 360 $m^2\ g^{-1}$, 0.948 $cm^3\ g^{-1}$, and 2.45 nm, respectively, by Brunauer–Emmett–Teller (BET) measurement (Figure 1c). The mass ratio of SWNT and MS was measured to be 0.227:1 by UV–Vis–NIR absorption spectra and Inductively Coupled Plasma-Mass Spectrometry (ICP-MS).

Thanks to the PEG coating, our SWNT@MS-PEG nanocomposite was water-soluble and exhibited excellent stability in various physiological solutions including phosphate buffered saline (PBS), and serum (**Figure 2**a). Moreover, the surface MS encapsulation and PEG modification did not affect the optical absorption property of SWNTs (Figure 2a). Strong resonance Raman scattering was also observed for the SWNT@MS-PEG sample, indicating that the chemical structure of nanotubes was largely intact after several steps of modifications (Supporting Information Figure S1b). As expected, when irradiated by an 808 nm NIR laser (0.7 W cm^{-2}), the SWNT@MS-PEG solution exhibited an obvious concentration-dependent heating effect (Figure 2b), allowing it to be effectively used as a photothermal agent.

Next, DOX was used as a model drug to test the potential of SWNT@MS-PEG as a DDS. The UV–Vis–NIR absorption

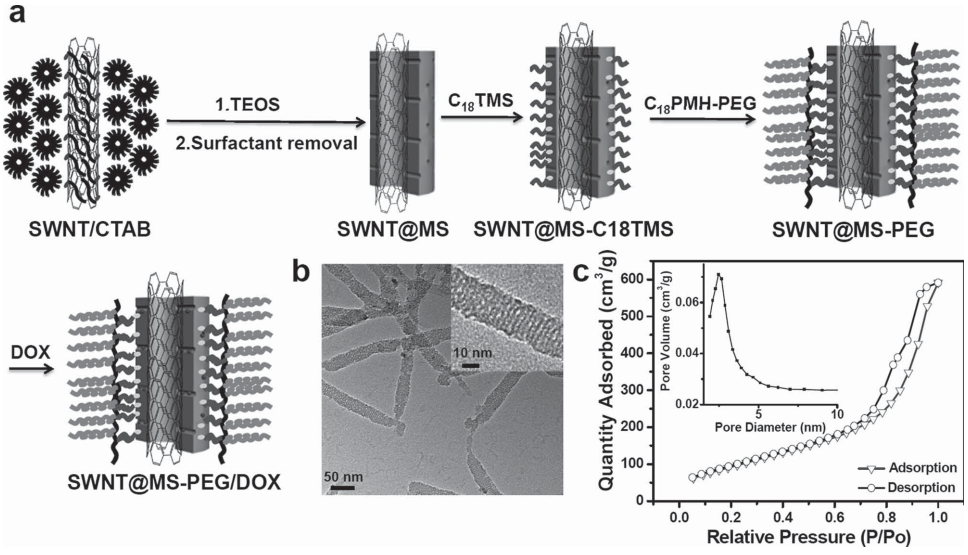

Figure 1. Preparation and characterization of SWNT@MS-PEG. a) A schematic illustration for the synthesis of SWNT@MS-PEG as well as drug loading. b) A TEM image of SWNT@MS. Inset is a TEM image with higher resolution. c) N_2 adsorption/desorption isotherms and corresponding pore-size distribution curve (inset) of the SWNT@MS sample.

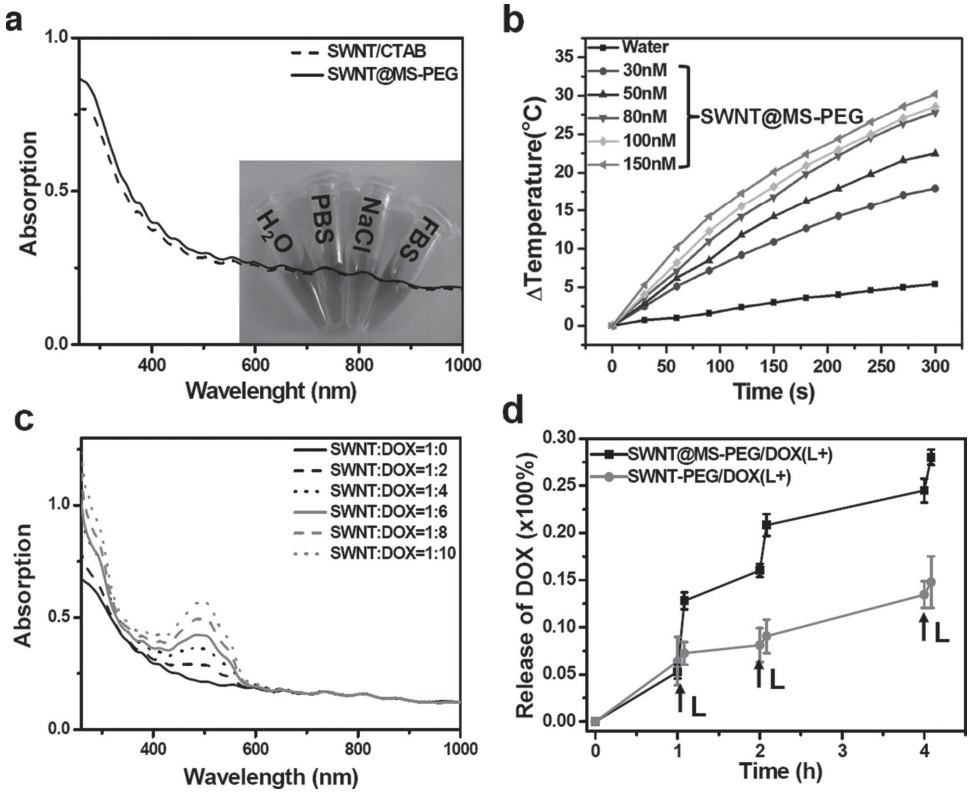

Figure 2. Drug loading and release. a) UV–Vis–NIR spectra of CTAB suspended SWNTs and SWNT@MS-PEG solutions at the SWNT concentration of 30 nM. Inset: a photo of SWNT@MS-PEG (30 nM) in different solutions. b) Temperature change curves of the SWNT@MS-PEG solution at different concentrations exposed to the 808 nm laser at a power density of 0.7 W cm^{-2} for 5 min. c) UV–Vis–NIR spectra of SWNT@MS-PEG loaded DOX with concentration of added DOX varying from 0 to 0.5 mg mL^{-1}. d) The NIR irradiation triggered release of DOX from SWNT@MS-PEG/DOX and SWNT-PEG/DOX in pH 7.4 PBS.

spectra of SWNT@MS-PEG/DOX samples obtained with different concentrations of DOX loading showed the characteristic absorption peak of DOX at ≈490 nm (Figure 2c), based on which the DOX loading on SWNT@MS-PEG was determined. It was measured that the DOX loading efficiency increased with the increasing amount of added DOX (Supporting Information Figure S2a), and reached the maximal loading capacity (DOX:SWNT = 5.7:1) when the mass ratio of added DOX to SWNT was 10:1. Further increase of added DOX concentration would lead to reduced stability of the final product (e.g., obvious aggregation). A moderate DOX loading (DOX:SWNT ≈ 2.3:1 in the final composite) was chosen in the following experiments.

It has been reported that many aromatic drug molecules including DOX could be directly adsorbed onto the outer-wall of SWNTs via hydrophobic interaction and π–π stacking.[16] In our SWNT@MS-PEG system, DOX is loaded inside the mesoporous silica structure without having strong contact with the SWNT wall. We next wondered whether the drug release behavior of DOX loaded SWNT@MS-PEG would be different from that of DOX loaded SWNT-PEG. Two samples, SWNT@MS-PEG/DOX and SWNT-PEG/DOX with the same SWNT and DOX concentrations were incubated in PBS at pH = 7.4 (Figure 2d). Several pulses of NIR laser irradiation (808 nm, 0.7 W cm^{-2}, 5 min for each pulse) were applied on those samples. The cumulative release of DOX was then measured based on UV–Vis–NIR absorption at various time points. For DOX directly adsorbed on SWNT-PEG, its release was not notable affect by NIR laser irradiation. Therefore, although PEGylated SWNTs themselves could serve as a drug carrier, their responsiveness to NIR light is rather weak. In marked contrast, SWNT@MS-PEG/DOX showed obvious burst drug release during the laser pulse, demonstrating much better sensitivity towards light stimulation. Such distinctive light-triggered drug release behaviors between two systems may likely be attributed to their different drug loading mechanisms. In SWNT@MS-PEG/DOX, DOX molecules are encapsulated inside mesoporous structure of the MS shell possibly with a weaker interaction compared to the π–π stacking between DOX and nanotube surface in the SWNT-PEG/DOX complex. The drug release in the latter case appears to be less sensitive to temperature change, while in the former case photothermal heating could instantly trigger DOX release from pores as also seen in many other MS coated nanostructure.[11,12] Moreover, the cumulative DOX release from SWNT@MS-PEG and SWNT-PEG in PBS buffer with different pH values were also investigated (Supporting Information Figure S2b), showing a higher cumulative DOX release at a lower pH, and a faster DOX releasing rate from SWNT@MS-PEG/DOX than that from SWNT-PEG/DOX.

We then tested the potential cytotoxicity SWNT@MS-PEG nanoplatform towards different types of cells. Three cells lines, 4T1 murine breat cancer cells, HeLa human cervical cancer

cells and 293T human embryonic kidney cells, were chosen to verify the safety of SWNT@MS-PEG. No obvious cytotoxicity was observed when the cells were incubated with various concentrations of SWNT@MS-PEG for 48 h (Supporting Information Figure S3a). Without surprise, DOX loaded SWNT@MS-PEG, on the other hand, was able to kill cancer cells by a concentration-dependent manner (Supporting Information Figure S3b).

Next, we wondered whether the NIR light trigger drug release behavior of SWNT@MS-PEG/DOX would also exist inside cells. Firstly, 4T1 cells were incubated with SWNT@MS-PEG/DOX for 1 h and then washed with fresh cell culture to remove nano-carriers and drugs outside cells. After being irradiated by the 808 nm laser at the power intensity of 0.4 W cm^{-2} for 20 min, the cells were imaged under a confocal fluorescence microscope (**Figure 3**a). Owing to the fluorescence quenching of DOX after loading on the SWNT@MS-PEG (Supporting Information Figure S4), the reoccurrence of DOX fluorescence could be an indicator of drug release. From the confocal fluorescence images (Figure 3b), no dramatic discrepancy was found in free DOX treated cells after laser irradiation, and the drug molecules were uniformly distributed in the cytoplasm and nuclei. In contrast, remarkably enhanced DOX fluorescence was observed in the cells incubated with SWNT@MS-PEG/DOX post laser exposure, suggesting release of DOX from the nano-carriers. Interestingly, obvious DOX fluorescence was noted inside cell nuclei for SWNT@MS-PEG/DOX incubated cells after laser irradiation as a result of drug release, but not for those without light exposure. Additionally, the quantitative data of flow cytometery further verified that the photothermal effect of SWNTs could enhance the intracellular release of DOX from nanocarriers (Supporting Information Figure S5). Our results collectively evidenced that NIR laser irradiation could effective release intracellular drug release of SWNT@MS-PEG/DOX.

The combination of photothermal with chemotherapy both delivered by SWNT@MS-PEG/DOX was then tested in vitro. In our experiments, 4T1 cells were incubated with SWNT@MS-PEG/DOX, SWNT@MS-PEG, and free DOX for 1 h, washed with fresh cell medium, and then irradiated with the 808 nm laser at different power densities for 20 min. Afterwards, the cells were re-incubated for additional 24 h before the MTT assay (Figure 3c). It was found that SWNT@MS-PEG/DOX treated cells showed remarkably reduced viabilities as the increase of laser power intensities, while the free DOX induced cancer cell killing was not significantly affected by laser irradiation. Simple photothermal heating induced by SWNT@MS-PEG without chemotherapy, on the other hand, appeared to be much less effective compared to the combination therapy, especially under lower laser powers. Therefore, it is concluded that NIR-light triggered intracellular drug release in such combined photothermal and chemotherapy could offer an obvious synergistic effect to destruct cancer cells.

Before moving forward to study in vivo tumor combination therapy by using SWNT@MS-PEG/DOX, we firstly studied the in vivo behaviors of such agent in animals utilizing the intrinsic

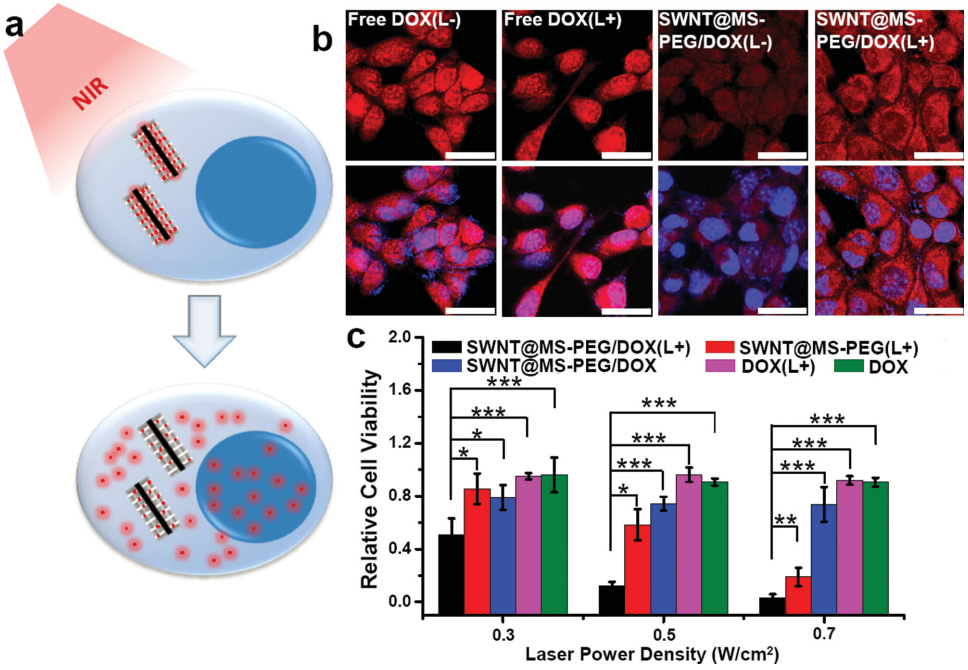

Figure 3. NIR-triggered intracellular drug release. a) A scheme showing NIR-triggered drug release from SWNT@MS-PEG/DOX in vitro. The uncovered DOX fluorescence from its quenched state inside SWNT@MS-PEG/DOX could be an indicator of drug release. b) Confocal fluorescence images of 4T1 cells incubated with SWNT@MS-PEG/DOX (or free DOX) ([DOX] = 25 μM) for 1h, washed with PBS to remove extracellular nanoparticles, and then treated with laser irradiation (808 nm, 0.4 W cm^{-2}, 20 min) (L+). Un-irradiated cells were used as the controls (L–). Red and blue colors represent DOX fluorescence and DAPI stained cell nuclei, respectively. The scale bar: 25 μm. c) Relative viabilities of 4T1 cells after various treatments. In this experiment, 4T1 cells were incubated with SWNT@MS-PEG/DOX(L+), SWNT@MS-PEG(L+), SWNT@MS-PEG/DOX, DOX(L+) and free DOX ([DOX] = 25 μM), for 1 h, and then wash with fresh cell culture and irradiated with the 808 nm laser at different power densities for 20 min. Afterwards cells were re-incubated for additional 24 h before the MTT assay. *P* values were calculated by Tukey's post-test (***p <0.001, **p <0.01, or *p <0.05).

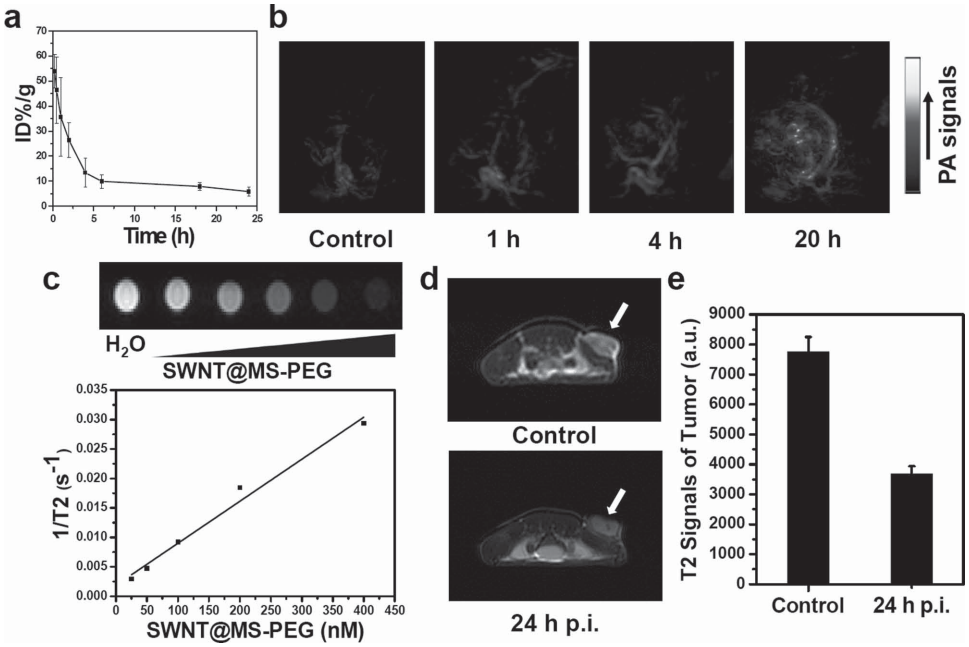

Figure 4. In vitro and in vivo photoacoustic and MR imaging. a) Blood circulation data of SWNT@MS-PEG/DOX after intravenous injection. SWNTs levels (in the unit of%ID/g) in the blood were measured by the Raman spectroscopy method. Error bars were based on triplicated samples. b) 2D photoacoustic imaging of tumors before and after injection of SWNT@MSN-PEG/DOX taken at different time points. c) T2-weighted MR images and T2 relaxation rates (R2) of SWNT@MS-PEG aqueous solutions at different SWNT concentrations. An obvious concentration-dependent darkening effect was observed in T2-weighted MR images. d) In vivo T2-weighted MR images of a mouse taken before injection (upper) and 24 h post injection (bottom). Obvious darkening effect showed up in the tumor after i.v. injection of SWNT@MS-PEG/DOX. e) T2-weighted MR signals of untreated and 24 h post injection tumors.

physical properties of SWNTs[22] Blood was extracted from Balb/c mice intravenous (i.v.) injected SWNT@MS-PEG/DOX ([SWNT]:4.3 mg kg^{-1}, [DOX]:10 mg kg^{-1}) at various time points post injection (p.i.). The concentrations of nanocomposite in the blood were determined by measuring the Raman signals of SWNTs. As shown in **Figure 4**a, the blood level of SWNT@MS-PEG/DOX decreased gradually over time. The SWNT signals in the blood remained at a reasonably high level even at 24 h post injection (p.i.).

In vivo multimodal imaging on mice injected with SWNT@MS-PEG/DOX was then carried out. SWNTs with strong NIR absorbance have previously been demonstrated to be an excellent contrast agent in photoacoustic (PA) imaging, which is a recently emerged imaging modality with improved tissue penetration and in vivo spatial resolution compared to traditional optical imaging techniques.[23,24] In our experiments, PA imaging was carried out in order to visualize the tumor microstructures (e.g., vasculature structures) and understand the intratumor distribution of nanoparticles at a high spatial resolution (Figure 4b). Mice bearing subcutaneous 4T1 tumors were i,v, injected with SWNT@MS-PEG/DOX. The blood vasculature, which was also seen before injection of SWNT@MS-PEG/DOX, showed enhanced PA signals after injection of our nanoagent. As the time passed, accumulation of nanoparticles inside the tumor was observed, as evidenced by the emergence of PA signals throughout the whole tumor at 24 h p.i.

In our and many others' previous studies,[18,25,26] it has been demonstrated that metallic nanoparticles anchored on SWNTs produced by the high-pressure CO disproportionation method (Hipco) could offer strong contrast in magnetic resonance (MR) imaging. As expected, an obvious concentration dependent darkening effect was observed in vitro T2-weighted MR images of our SWNT@MS-PEG sample, indicating its potential use in T2-weighted MR imaging (Figure 4c). After i.v. injection of SWNT@MS-PEG/DOX into 4T1 tumor-bearing mice, remarkably darken appearance was observed in the tumor region of mice from in vivo MR imaging, suggesting high tumor accumulation of those nanoparticles after systemic administration (Figure 4d). The quantitative MR imaging results based on region-of-interest (ROI) quantification[23] further verify the T2 signals were obviously decreased in the tumor region after i.v. injection of SWNT@MS-PEG for 24 hours (Figure 4e). Therefore, both in vivo PA imaging and MR imaging verified the efficient tumor homing of SWNT@MS-PEG/DOX after i.v. injection.

Inspired by the fascinating in vitro synergistic therapeutic effect and the efficient tumor accumulation of SWNT@MS-PEG/DOX, we then conducted the animal experiments to realize the chemo-photothermal combination therapy in vivo by using SWNT@MS-PEG/DOX. 4T1 tumor modal on Balb/c mice was developed by subcutaneously injecting 1×10^6 murine breast cancer 4T1 cells into the back of each Balb/c mouse.[27] When the tumor size reached about 60 mm^3, mice were divided into different groups (5 mice per group) and i.v. injected with SWNT@MS-PEG/DOX, SWNT@MS-PEG, DOX, PBS respectively ([SWNT]:4.3 mg kg^{-1}, [DOX]:10 mg kg^{-1}). At 24 h p.i., their tumors were irradiated by the 808 nm laser at a moderate power density of 0.5 W cm^{-2} for 20 min.

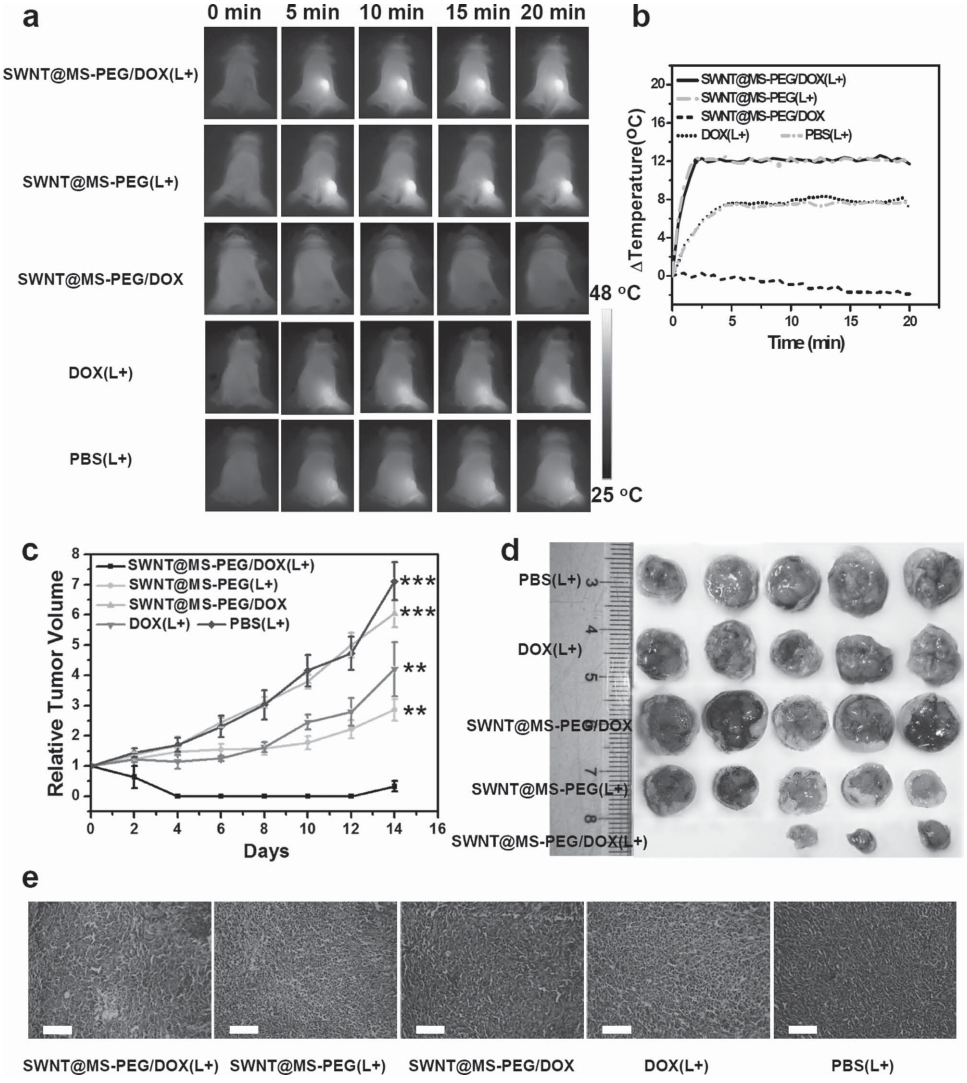

Figure 5. In vivo combination therapy by using SWNT@MS-PEG/DOX. a) IR thermal images of 4T1 tumor-bearing mice recorded by an IR camera. The doses of DOX and SWNT@MS-PEG were 10 mg kg^{-1} and 4.3 mg kg^{-1}, respectively, in this experiment. Laser irradiation was conducted by using 808 nm NIR laser at the power density of 0.5 W cm^{-2} for 20 min on the tumors. b) Temperature changes of tumors monitored by the IR thermal camera in different groups during laser irradiation as indicated in (a). c) Tumor growth curves of different groups of mice after various treatments indicated. Error bars were based on standard error of the mean (SEM) of five tumors per group. d) Photos of the tumors collected from different groups of mice at the end of treatments (day 14). Note that in the combination treatment group, 2 out of 5 tumors were completely eliminated after treatment. e) H&E-stained tumor slices collected from mice post various treatments indicated. The scale bar: 100 μm. *P* values in (c) were calculated by Tukey's post-test (***p <0.001, **p <0.01, or *p <0.05).

An IR thermal camera was used to monitor the tumor temperature (**Figure 5**a,b). It was found that the tumor surface temperatures of mice treated with SWNT@MS-PEG/DOX and SWNT@MS-PEG rapidly increased and maintained at ≈48 °C during laser irradiation. In contrast, the mice treated with PBS and DOX showed no apparently heating in the tumor region when irradiated by the laser.

After receiving various treatments, the tumor sizes were measured every 2 days by a digital caliper. Remarkably, the tumor growths on mice with injection of SWNT@MS-PEG/DOX were effectively inhibited after NIR laser irradiation as a result of the combined chemo-photothermal therapy (Figure 5c,d). Tumors on two out of five mice in this group were even completely eliminated post treatment. In marked contrast, neither photothermal therapy alone (SWNT@MS-PEG (L+)) nor chemotherapy (SWNT@MS-PEG/DOX) by itself could effectively inhibit the tumor growth, although the tumor development was slightly delayed after the mild photothermal heating in the SWNT@MS-PEG (L+) group. The efficacy of free DOX even under NIR laser irradiation also appeared to be limited because of the absence of photothermal effect in this group. Hematoxylin and eosin (H&E) staining of tumor slices (Figure 5e) further confirmed that while cells in control groups of tumors largely retained their normal morphology with distinctive membrane and nuclear structures, most tumor cells were severely destroyed in the group receiving both SWNT@MS-PEG/DOX

injection and NIR laser irradiation. Such dramatic synergistic effect may be explained by two mechanisms. Firstly, as revealed by many previous studies[28] and also uncovered in our own experiments (Supporting Figure S6), mild photothermal heating could increase the cell membrane permeability and significantly promote internalization of nano-carriers. In the meanwhile, the NIR-triggered drug release, especially from SWNT@MS-PEG/DOX inside cells, could further enhance the cell killing efficacy of chemotherapeutics.

At last, we examined potential toxic side effect of such combination therapy offered by SWNT@MS-PEG/DOX. Notably, all mice behaved normally after receiving various treatments (Supporting Information Figure S7). Histology analysis (Supporting Figure S8) of major organs from mice 14 days after SWNT@MS-PEG/DOX injection and laser treatment indicated no appreciable abnormality or noticeable organ damages. Those preliminary results verified that our SWNT@MS-PEG/DOX rendered no obvious toxic side effect to the mice in the short term at our tested dose.

3. Conclusions

In conclusion, we present a multifunctional nanoplatform based on PEGylated, MS coated SWNTs, which could simultaneous serve as a drug loading carrier, a NIR photothermal heater, and a multimodal imaging probe, useful for imaging and combination therapy of cancer. Unlike previously developed SWNT-drug complex, SWNT@MS-PEG/DOX exhibits rapid NIR light-triggered drug release behavior, which can be utilized to enhance the cancer cell killing by chemotherapeutics. Owing to the efficient tumor accumulation as revealed by in vivo bimodal PA and MR imaging, in vivo combination therapy is then carried out, realizing an outstanding tumor growth inhibition effect by a single treatment in an animal tumor model upon systemic administration of SWNT@MS-PEG/DOX. Compared with other previously reported MS coated photothermal agents (e.g., MS coated gold nanorods, graphene oxide, etc.), SWNTs are unique in their highly enriched intrinsic imaging functions that enable multimodal PA and MR imaging as conducted in this work, as well as Raman and NIR-II fluorescence imaging,[25] which although demonstrated here could provide additional values to visualized medicine. Further surface engineering of those nanostructures may allow active tumor targeting and more precisely controlled drug release under other stimuli in addition to NIR light, to achieve cancer therapy with even better specificity, a long-term goal in our laboratory.

4. Experimental Section

Materials: All chemicals, unless specified otherwise, were purchased from Sigma-Aldrich and used as received. PEG polymers were purchased from PegBio, Suzhou, China. All cell-culture related reagents were purchased from Hyclone. Female Balb/c mice were purchased from Nanjing Peng Sheng Biological Technology Co. Ltd.

Synthesis of Mesoporous Silica Coated SWNTs: CTAB suspended SWNTs were prepared by sonicating SWNTs (1 mg mL^{-1}) in a solution of CTAB (10 mg mL^{-1}) for 5 h,[19,29] yielding a black suspension which was then centrifuged at about 14 800 rpm for 1 h at 10 °C to remove the deposite and most of the crystallized CTAB. To synthesis silica coated SWNTs, 0.5 mL of the SWNT dispersion, 2 mL of H_2O, 1 mL of CTAB/H_2O (1 mg mL^{-1}), and 1 mL of NaOH aqueous solution (0.01 M) were added in a vial and ultrasonicated for 10 minutes. Under 60 °C, 50 µL of TEOS/ethanol (v/v = 1/4) solution was injected into the vial. After shaking mildly for 30 minutes, this vial was heated at 60 °C without stirring for 12 h. Then the solid product was washed with ethanol for 3–4 times under centrifugation to remove the mesostructural template CTAB to form SWNT@MS following the literature procedure.[10,19] The yielded SWNT@MS with CTAB removed could not be re-dispersed in water, suggesting that the majority of CTAB was removed after ethanol washing.

PEGylation of SWNT@MS: 20 µL of C18TMS solution in chloroform (30%) was added into the solution of SWNT@MS in ethanol drop-by-drop during stirring. Then the mixed solution was stirred for 18 h. C18TMS modified SWNT@MS were washed with ethanol for three times at the speed of 14800 rpm and then dispersed in chloroform. For PEGylation, C18PMH-PEG polymer was synthesized according to a previous report.[30] 5 mL of SWNT@MS-C18TMS chloroform solution was mixed with 200 µL chloroform solution containing 5 mg C18PMH-PEG and stirred overnight at room temperature. After slow evaporation of chloroform under low-pressure, a dry film of nanoparticles was obtained and then dispersed into by distilled (DI) water. To remove the excess polymer, the solution was washed with DI water repeatedly, obtaining purified SWNT@MS-PEG sample which was redispersed in DI water. The molar concentration of SWNTs was determined by their absorbance at 808 nm with a molar extinction co-efficient at 7.9×10^6 cm^{-1} M^{-1}.[31] PEGylated SWNTs (SWNT-PEG) were synthesized according to our well-established protocol by sonciating SWNTs (0.2 mg/mL) in a solution of C18PMH-PEG (2 mg/mL) for 1 h, centrifugation at 24 000 g for 1 h to remove the precipitates, and filtration through 0.1 µm membrane filter to remove excess polymer.[25]

Characterization: Transmission electron microscopy (TEM) and high-resolution TEM (HR-TEM) images were obtained using a Philips CM300 transmission electron microscope operating at an acceleration voltage of 200 kV. UV–Vis–NIR absorption spectra were recorded with a GENESYS 10S UV–Vis spectrophotometer. Laser irradiation was performed using an optical-fiber-coupled power-tunable diode laser (continuous wave) (maximal power = 10 W, Hi-Tech Optoelectronics Co., Beijing, China). The Brunauer-Emmett-Teller (BET) surface area and pore size were measured using ASAP2050 system.

Drug Loading and Releasing: For drug loading,[32] the SWNT@MS-PEG (300 nM) was mixed with different concentrations of DOX (0.1–0.5 mg mL^{-1}) in phosphate buffer (PBS, 20 mM) at pH = 8.0. Unbound excess DOX was removed by ultra-filtration through a 100 kDa filter and washed thoroughly with water until the filtrate was nearly colorless. The DOX loading capacities were calculated by measuring the UV–Vis–NIR spectra of the SWNT@MS-PEG before and after loading DOX. The formed SWNT@MS-PEG/DOX complex was stored at 4 °C. To study the release of DOX, SWNT@MS-PEG/DOX and SWNT-PEG/DOX solutions in pH 7.4 PBS were irradiated with the 808 nm laser for 5 min with the power density at 0.7 W cm^{-2}. The released DOX was removed by ultra-filtration. UV–Vis–NIR spectra of SWNT@MS-PEG/DOX before and after laser irradiation were measured to determine the amount of released DOX.

Cell Culture Experiments: 4T1, HeLa, and 293T cells originally obtained from American Type Culture Collection (ATCC) were cultured at 37 °C under 5% CO_2. All cell culture related reagents were purchased from Invitrogen. Confocal fluorescence imaging of cells was performed using a Leica SP5 laser scanning confocal microscope. Flow cytometry measurement was conducted by BD FACS Calibur (Bectone Dickinson).

Cytotoxicity Assays: 4T1, HeLa, and 293T cells pre-seeded in 96-well plates at 1×10^4/well were incubated with different concentrations of SWNT@MS-PEG, SWNT@MS-PEG/DOX or free DOX for desired periods of time. Afterwards, the cells were washed with fresh cell culture medium, The standard cell viability MTT assay was carried out to determine the cell viabilities relative to the untreated control.

Intracellular Drug Release: To investigate the NIR-triggered intracellular drug release, 4T1 cells were incubated with SWNT@MS-PEG/DOX or free DOX at the same concentration of DOX (25 µM) for 1h, then treated

with or without irradiation by the 808 nm laser for 20 min under the power density about 0.4 W cm^{-2}. All cells were washed twice with PBS before confocal imaging (LeciaSP5 laser scanning confocal microscope). The fluorescence of DOX (emission range 500 to 700 nm) was excited by using a 488 nm laser. Those cells were also analyzed by flow cytometry using a Calibur flow cytometer (BD Biosciences, USA).

In Vitro Combination Therapy: For combination therapy, 4T1 cells were treated with SWNT@MS-PEG/DOX (L+) SWNT@MS-PEG/DOX, SWNT@MS-PEG (L+), DOX (L+) and DOX ([DOX] = 25 μM) for 1 h, washed with fresh cell medium and then irradiated by a 808 nm NIR laser at the power densities of 0.3 W cm^{-2}, 0.5 W cm^{-2}, 0.7 W cm^{-2} for 20 min. After additional incubation for 24 h, the relative cell viabilities were then measured by the MTT assay.

In Vivo Combination Therapy: All animal experiments were carried out under protocols approved by Soochow University Laboratory Animal Center. To develop the tumor model, 4T1 cells (1×10^6) suspended in 40 μL of PBS were subcutaneously injected into the back of each mouse. After the tumor volumes reached ≈60 mm^3, mice were divided into five groups with five mice per group. Each group of mice were i.v. injected with 200 μL of PBS, DOX, SWNT@MS-PEG/DOX, or SWNT@MS-PEG ([DOX]:10 mg kg^{-1}, [SWNT]:4.3 mg kg^{-1}). After 24 h, the tumors were treated with or without NIR light (0.5 W cm^{-2}, 808 nm). An IR thermal camera (Infrared Cameras. Inc.) was used to record temperature changes during laser irradiation. After treatments, the length and width of the tumors were monitored by a digital caliper every 2 days for 2 weeks. The tumor volume was calculated according to the following formula: $width^2 \times length/2$.

In Vivo Imaging: 4T1 tumor-bearing mice were i.v. injected with SWNT@MS-PEG/DOX ([DOX]:10 mg kg^{-1}, [SWNT]:4.3 mg kg^{-1}) for in vivo PA and MR imaging. PA imaging was performed with a preclinical photoacoustic computed tomography scanner (Endra Nexus 128, Ann Arbor, MI). During our experiments, anesthesia was maintained using pentobarbital (50 mg kg^{-1}). The body temperature of the mice was maintained by using a water heating system at 37.5 °C. MR imaging of mice was accomplished with the 3 T clinical MRI scanner (Bruker Biospin Corporation, Billerica, MA, USA) equipped with a special coil used for small-animal imaging.

Blood Circulation: 200 μL of SWNT@MS-PEG/DOX ([DOX]:10 mg kg^{-1}, [SWNT]:4.3 mg kg^{-1}) saline solution was i.v. injected via the tail vein into each mouse. At various time points p.i., about 20 μL of blood was sampled from each mouse and dissolved in 80 μL of lysis buffer (1% SDS, 1%Triton X-100, 40 mM Tris acetate, 10 mM EDTA, 10 mM DTT). Raman spectra of the lyzed blood samples were recorded under 785 nm excitation to determine SWNT levels in the blood based on the characteristic Raman signals from SWNTs (the G-band peak). The percent injected dose per gram (%ID/g) of blood was calculated by the following equation:

$$\%ID/g = [SWNT]_{bloodlysate} \times V_{bloodlysate} / ([SWNT]_{injected} \times V_{injectedSWNT} \times bloodweight) \times 100\% \quad (1)$$

Acknowledgements

This work was partially supported by the National Basic Research Programs of China (973 Program) (2012CB932600, 2011CB911002), the National Natural Science Foundation of China (51222203, 51132006), a Jiangsu Natural Science Fund for Distinguished Young Scholars, the Jiangsu Key Laboratory for Carbon-Based Functional Materials & Devices, and a Project Funded by the Priority Academic Program Development (PAPD) of Jiangsu Higher Education Institutions. The authors thank Prof. Gang Liu from Xiamen University for his kind help in photoacoustic imaging.

Received: September 6, 2014
Revised: October 20, 2014
Published online: November 20, 2014

[1] a) K. L. Donaldson, G. L. Goolsby, A. F. Wahl, *Int. J. Cancer* **1994**, *57*, 847; b) D. N. Carney, J. B. Mitchell, T. J. Kinsella, *Cancer Res.* **1983**, *43*, 2806.
[2] a) W. Arap, R. Pasqualini, E. Ruoslahti, *Science* **1998**, *279*, 377; b) T.-Y. Liu, S.-H. Hu, T.-Y. Liu, D.-M. Liu, S.-Y. Chen, *Langmuir* **2006**, *22*, 5974.
[3] a) Y. Chen, H. Chen, J. Shi, *Adv. Mater.* **2013**, *25*, 3144; b) G. Yang, H. Gong, X. Qian, P. Tan, Z. Li, T. Liu, J. Liu, Y. Li, Z. Liu, *Nano Res.* **2014**, DOI: 10.1007/s12274–014–0558–0.
[4] a) D. He, X. He, K. Wang, J. Cao, Y. Zhao, *Adv. Funct. Mater.* **2012**, *22*, 4704; b) J. Liu, W. Bu, L. Pan, J. Shi, *Angew. Chem. Int. Ed.* **2013**, *52*, 4375.
[5] a) S. Angelos, Y.-W. Yang, K. Patel, J. F. Stoddart, J. I. Zink, *Angew. Chem.* **2008**, *120*, 2254; b) N. Wang, Z. Zhao, Y. Lv, H. Fan, H. Bai, H. Meng, Y. Long, T. Fu, X. Zhang, W. Tan, *Nano Res.* **2014**, DOI: 10.1007/s12274–014–0493–0.
[6] Y.-Z. You, K. K. Kalebaila, S. L. Brock, D. Oupický, *Chem Mater.* **2008**, *20*, 3354.
[7] J. Li, F. Liu, Q. Shao, Y. Min, M. Costa, E. K. L. Yeow, B. Xing, *Adv. Healthcare Mater.* **2014**, *3*, 1230.
[8] a) R. Liu, X. Zhao, T. Wu, P. Feng, *J. Am. Chem. Soc.* **2008**, *130*, 14418; b) C.-Y. Lai, B. G. Trewyn, D. M. Jeftinija, K. Jeftinija, S. Xu, S. Jeftinija, V. S. Y. Lin, *J. Am. Chem. Soc.* **2003**, *125*, 4451; c) Z. Luo, Y. Hu, K. Cai, X. Ding, Q. Zhang, M. Li, X. Ma, B. Zhang, Y. Zeng, P. Li, J. Li, J. Liu, Y. Zhao, *Biomaterials* **2014**, *35*, 7951.
[9] a) Y. Chen, H. Chen, S. Zhang, F. Chen, L. Zhang, J. Zhang, M. Zhu, H. Wu, L. Guo, J. Feng, J. Shi, *Adv. Funct. Mater.* **2011**, *21*, 270; b) G. Terentyuk, E. Panfilova, V. Khanadeev, D. Chumakov, E. Genina, A. Bashkatov, V. Tuchin, A. Bucharskaya, G. Maslyakova, N. Khlebtsov, B. Khlebtsov, *Nano Res.* **2014**, *7*, 325.
[10] Z. Zhang, L. Wang, J. Wang, X. Jiang, X. Li, Z. Hu, Y. Ji, X. Wu, C. Chen, *Adv. Mater.* **2012**, *24*, 1418.
[11] S. Shen, H. Tang, X. Zhang, J. Ren, Z. Pang, D. Wang, H. Gao, Y. Qian, X. Jiang, W. Yang, *Biomaterials* **2013**, *34*, 3150.
[12] Y. Wang, K. Wang, J. Zhao, X. Liu, J. Bu, X. Yan, R. Huang, *J. Am. Chem. Soc.* **2013**, *135*, 4799.
[13] G. Song, Q. Wang, Y. Wang, G. Lv, C. Li, R. Zou, Z. Chen, Z. Qin, K. Huo, R. Hu, J. Hu, *Adv. Funct. Mater.* **2013**, *23*, 4281.
[14] a) H.-M. So, K. Won, Y. H. Kim, B.-K. Kim, B. H. Ryu, P. S. Na, H. Kim, J.-O. Lee, *J. Am. Chem. Soc.* **2005**, *127*, 11906; b) X. Wang, C. Wang, L. Cheng, S.-T. Lee, Z. Liu, *J. Am. Chem. Soc.* **2012**, *134*, 7414; c) Z. Liu, K. Chen, C. Davis, S. Sherlock, Q. Cao, X. Chen, H. Dai, *Cancer Res.* **2008**, *68*, 6652; d) N. W. S. Kam, Z. Liu, H. Dai, *Angew. Chem.* **2006**, *118*, 591; e) D. Tasis, N. Tagmatarchis, A. Bianco, M. Prato, *Chem. Rev.* **2006**, *106*, 1105.
[15] Z. Liu, X. Li, S. M. Tabakman, K. Jiang, S. Fan, H. Dai, *J. Am. Chem. Soc.* **2008**, *130*, 13540.
[16] Z. Liu, X. Sun, N. Nakayama-Ratchford, H. Dai, *ACS Nano* **2007**, *1*, 50.
[17] X. Liu, H. Tao, K. Yang, S. Zhang, S.-T. Lee, Z. Liu, *Biomaterials* **2011**, *32*, 144.
[18] C. Wang, X. Ma, S. Ye, L. Cheng, K. Yang, L. Guo, C. Li, Y. Li, Z. Liu, *Adv. Funct. Mater.* **2012**, *22*, 2363.
[19] K. Ding, B. Hu, Y. Xie, G. An, R. Tao, H. Zhang, Z. Liu, *J. Mater. Chem.* **2009**, *19*, 3725.
[20] R. K. Singh, K. D. Patel, J.-J. Kim, T.-H. Kim, J.-H. Kim, U. S. Shin, E.-J. Lee, J. C. Knowles, H.-W. Kim, *ACS Appl. Mater. Inter.* **2014**, *6*, 2201.
[21] R. Huang, L. Han, J. Li, S. Liu, K. Shao, Y. Kuang, X. Hu, X. Wang, H. Lei, C. Jiang, *Biomaterials* **2011**, *32*, 5177.
[22] Z. Liu, C. Davis, W. Cai, L. He, X. Chen, H. Dai, *Proc. Natl Acad Sci.* **2008**, *105*, 1410.
[23] Z. Li, S. Yin, L. Cheng, K. Yang, Y. Li, Z. Liu, *Adv. Funct. Mater.* **2014**, *24*, 2312.

[24] a) L. Cheng, J. Liu, X. Gu, H. Gong, X. Shi, T. Liu, C. Wang, X. Wang, G. Liu, H. Xing, W. Bu, B. Sun, Z. Liu, *Adv. Mater.* **2014**, *26*, 1886; b) D. Chen, C. Wang, X. Nie, S. Li, R. Li, M. Guan, Z. Liu, C. Chen, C. Wang, C. Shu, L. Wan, *Adv. Funct. Mater.* **2014**, DOI: 10.1002/adfm.201401560; c) M. Xu, L. V. Wang, *Rev. Sci. Instrum.* **2006**, *77*, 041101.
[25] C. Liang, S. Diao, C. Wang, H. Gong, T. Liu, G. Hong, X. Shi, H. Dai, Z. Liu, *Adv. Mater.* **2014**, *26*, 5646.
[26] Z. Liu, W. Cai, L. He, N. Nakayama, K. Chen, X. Sun, X. Chen, H. Dai, *Nat. Nanotechnol.* **2007**, *2*, 47.
[27] T. Liu, C. Wang, X. Gu, H. Gong, L. Cheng, X. Shi, L. Feng, B. Sun, Z. Liu, *Adv. Mater.* **2014**, *26*, 3433.
[28] a) B. Tian, C. Wang, S. Zhang, L. Feng, Z. Liu, *ACS Nano* **2011**, *5*, 7000; b) C. Wang, H. Xu, C. Liang, Y. Liu, Z. Li, G. Yang, L. Cheng, Y. Li, Z. Liu, *ACS Nano* **2013**, *7*, 6782; c) L. Feng, X. Yang, X. Shi, X. Tan, R. Peng, J. Wang, Z. Liu, *Small* **2013**, *9*, 1989.
[29] J. Liu, W. Bu, S. Zhang, F. Chen, H. Xing, L. Pan, L. Zhou, W. Peng, J. Shi, *Chem. Eur J.* **2012**, *18*, 2335.
[30] C. Wang, L. Cheng, Z. Liu, *Biomaterials* **2011**, *32*, 1110.
[31] N. W. S. Kam, M. O'Connell, J. A. Wisdom, H. Dai, *Proc. Natl. Acad. Sci. U.S.A.* **2005**, *102*, 11600.
[32] Z. Liu, A. C. Fan, K. Rakhra, S. Sherlock, A. Goodwin, X. Chen, Q. Yang, D. W. Felsher, H. Dai, *Angew. Chem. Int. Ed.* **2009**, *48*, 7668.